Discover Sustainability

Research

Geospatial analysis of unplanned urbanization: impact on land surface temperature and habitat suitability in Cuttack, India

Prasanta Kumar Patra[1] · Duryadhan Behera[1] · Vishal Chettry[2] · Krishna Manjari Jena[1] · Shreerup Goswami[3] · Muralitharan Jothimani[4]

Received: 12 December 2024 / Accepted: 11 February 2025
Published online: 19 February 2025

Abstract
Unplanned urbanization causes an increase in land surface temperature (LST) and adversely affects the climate and environment within cities. Cuttack City, India, is experiencing rapid urbanization at an alarming rate, facing particular environmental challenges and hosting critical ecosystems that require protection. This study uses the Urban Growth Suitability Index (UGSI) to determine which parts of the city are Suitable and which are unsuitable for habitation based on the geographic distribution of heat vulnerability surrounding Cuttack City from 1990 to 2020. Using a mono window method, the LST for 1990, 2000, 2010, and 2020 is derived from the Landsat 5, Landsat 7, and Landsat 8 satellite data. A simple linear regression model has been used to establish a trend in the relationship between LST and land use/land cover (LULC), similar to UGSI with LST. Finally, the most Suitable and Unsuitable regions for habitation in Cuttack City are marked using UGSI. The findings indicate that the highest temperature in the city was 32.07 °C in 1990 and increased to 38.67 °C in 2020. This is due to the decrease in city vegetation area by 51.39% and the expansion of the urban area by 58.19%. The core region of the city shows higher temperatures than the urban fringes, where vegetation cover is scanty or has no greenery. Out of 59 administrative wards (Municipal administrative regions) in Cuttack City, 27 experienced acute temperatures due to sparse vegetation cover and an intense built environment. A total area of 15.99 km^2 of Cuttack City facing this heat vulnerability accounts for 19.61% of the total City area, which is highly unsuitable for habitation, and 10.77 km^2 of Cuttack City, which accounts for only 13.21% of the city area are Suitable for habitation. This study will help city planners by guiding actions to protect residents from the adverse effects of extreme heat. By combining thermal and land use analyses with the UGSI framework, this study offers a novel approach to spatially mapping heat vulnerability and urban growth suitability, enhancing urban planning strategies in rapidly urbanizing regions. However, the lack of high-resolution satellite data and the exclusion of socio-economic factors highlight the need for further research. Integrating finer-scale data could offer more robust insights for urban sustainability planning.

Keywords Cuttack city · Heat vulnerability · Land surface temperature · Remote sensing · Urban growth suitability index

✉ Muralitharan Jothimani, muralitharangeo@gmail.com | [1]Department of Earth Sciences, Sambalpur University, Burla, Odisha, India. [2]Department of Architecture, Planning and Design, Indian Institute of Technology (BHU), Varanasi, Uttar Pradesh, India. [3]Department of Geology, Utkal University, Bhubaneswar, Odisha, India. [4]Department of Geology, College of Natural and Computational Sciences, Arba Minch University, Arba Minch, Ethiopia.

1 Introduction

Rapid, unplanned urban expansion creates a significant threat to the urban ecosystem. Due to the country's population boom and economic prosperity, metropolitan regions in India have seen exponential growth in recent decades [1–3]. Unplanned urbanization increases LST, reduces green space in cities, and lowers groundwater levels [4–7]. Urbanization causes environmental issues, including increased urban Heat Island (UHI), climate change, urban hydrology, etc., since it changes LULC [8, 9]. The UHI is a prominent consequence of alterations in LULC primarily driven by human activities [10–12]. The UHI phenomenon refers to the situation in which urban areas exhibit higher air and LST than nearby rural areas [13, 14]. The consequences of UHI are attributed to an increase in the emission of greenhouse gases, air pollution, and energy consumption [15, 16].

The primary cause of the UHI effect is the landscape transformation resulting from extensive urban development [17, 18]. Naturally, vegetated areas are swapped with impervious areas like buildings, roads, and railways that block natural seepage of rainwater and trap incoming solar radiation to increase surface temperature. In addition to this, a rise in vehicular emissions and gas released from air conditioners and factories also contributed to this UHI effect. The UHI effect causes various diseases in city dwellers due to poor air quality and high temperatures [19, 20]. UHI has become a significant concern over the past five decades [17–21].

After Luke Howard's (1833) work on the UHI effect, many studies have been undertaken that show the cause and impact of the UHI effect [22, 23]. Similar studies on the effects of urbanization on the environment and their repercussions have recently been conducted using GIS and remote sensing [24–28]. These research findings demonstrate that anthropogenic-induced activities are solely responsible for the rise in city temperature, which brings serious health consequences [29–31]. Urbanization and the movement of people from rural to urban places pose significant challenges in India [32, 33]. According to a report released by the National Commission on Population (NCP), it is anticipated that by 2050, urban regions will be home to half of India's population (https://main.mohfw.gov.in). UN's goal for sustainable urban development emphasizes the promotion of sustainable cities and communities that can be achieved through implementing sustainable urban planning practices [9]. Much research has assessed how LULC modifications affect the UHI phenomenon. However, these studies have primarily focused on major Indian cities, leaving a gap in understanding the situation for smaller, rapidly growing cities, which can be somewhat alarming. Major cities in India, like Delhi, Bengaluru, Hyderabad, Chennai, and Kolkata, with populations above 5 million, have exceeded their capacity to accommodate people sustainably. Hence, cities with populations below 5 million experience significant expansion in their built-up environment. This unplanned urban growth resulted in urban sprawl and a rise in surface temperature in these medium-sized cities [34]. Hence, it is essential to observe and measure the urban growth and its impact on the increase in surface temperature in medium-sized Indian cities.

Medium-sized cities like Cuttack serve as critical case studies for understanding the dynamics of urbanization and its environmental consequences. These cities often experience rapid growth that outpaces their planning and infrastructure development, leading to significant environmental and climatic challenges. Unlike larger metropolitan areas, medium-sized cities typically lack the financial and institutional resources to implement advanced urban management strategies, making them more vulnerable to heat stress, urban sprawl, and ecological degradation. Cuttack City, the former capital of Odisha, India, is an ancient city with a significant role in the state's economy. It holds immense socio-economic potential, attracting migration from rural areas within the state and beyond. People migrated to Cuttack for its opportunities in education, healthcare, and an improved lifestyle, leading to a rise in unplanned city-built environments and slum areas. This rapid urban expansion directly impacts land use and land cover patterns of the city, leading to increased land surface temperatures (LST) and exacerbating heat vulnerability. Studying such cities offers valuable insights into how urbanization affects the environment at a scale that is often overlooked in global analyses.

This study addresses the urgent need to understand the environmental impacts of unplanned urban growth in Cuttack City. While prior research on Cuttack City has measured urban expansion and temporal LULC changes [12, 20], the environmental implications, particularly on temperature variation and urban heat vulnerability, remain underexplored. This study addresses that gap by evaluating the UGSI to identify suitable and unsuitable areas in Cuttack City for living based on extreme heat conditions.

To achieve this objective, this study examines Cuttack City's land use/ Land Cover changes and temperature variations over 30 years (1990–2020) using Landsat-5 TM, Landsat-7 ETM + , and Landsat-8 OLI/TIRS satellite images to extract LST over Cuttack City. Then, it employs these LSTs to find suitable and unsuitable areas (in terms of extreme

heat) within the city to live in by looking at the UGSI. This research aligns with Sustainable Development Goals (SDGs) by promoting environmental sustainability and climate action. It is valuable for informing the Indian government's Smart Cities Mission and aiding urban planners and policymakers in making well-informed decisions for sustainable urban development that consider local and global objectives.

2 Study area

Geographically, Cuttack City of Odisha is located at 20°27′53.89″N latitude and 85°52′45.37″E longitude (Fig. 1). The city, bisected by the Mahanadi and Kathojodi rivers, is partitioned into three sectors, encompassing a combined land area of 81.52 km^2 [35, 36]. Its strategic location has made it a vital hub for trade and commerce, resulting in high population densities within existing built-up land. As an industrial and economic center, Cuttack City attracts a growing workforce, further accelerating urban expansion. Additionally, the presence of key institutions such as SCB Medical College and Ravenshaw University has concentrated urban growth around these nodes, reflecting the city's role as an administrative, educational, and healthcare hub. For better governance, the city is divided into 59 administrative wards. Cuttack experiences a temperate climate, with an average annual rainfall of approximately 144 cm and summer temperatures ranging from 35 °C to 42 °C. According to the 2011 census, the city's population was 6.1 lakh, with the 2020 population interpolated based on this data. The Population density of the city has increased significantly from 4,948 in 1990 to 8,422 in 2020. This rise in population indeed triggers a change in the land cover of the town.

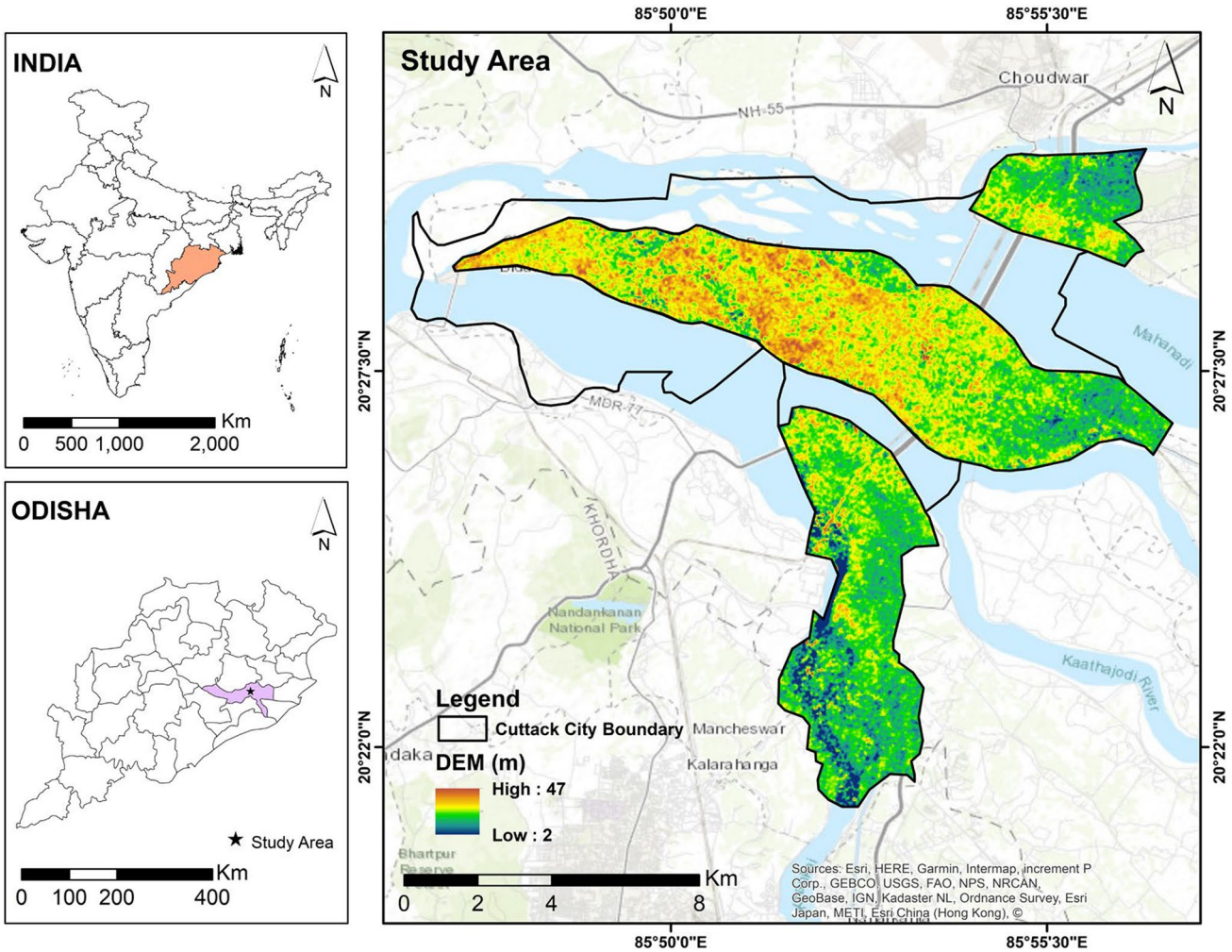

Fig. 1 Location Map

3 Data and methodology

For the temporal study of LULC change in Cuttack City, Landsat satellite data for the years 1990, 2000, 2010, and 2020, freely obtained from the USGS website, were downloaded and subsequently georeferenced in the WGS84 datum, followed by projection in UTM zone 45 N. The specification of satellite data is given in Table 1. Cuttack City boundary is collected from the Cuttack Municipal Corporation (CMC) website to prepare our study area boundary (https://cmccuttack.odisha.gov.in/). Population data for Cuttack City was collected from the Census of India handbook. All collected satellite data have less than 20% cloud cover to achieve a better result and minimize error. Arc GIS 10.2 software is used for analysis and map preparation. The adopted methodology is displayed in Fig. 2.

3.1 Pre-processing of satellite data

Initially, satellite data of Cuttack City for the years 1990, 2000, 2010, and 2020 is radiometrically and geometrically corrected for better accuracy. For atmospheric correction, the Darkest Pixel (DP) method, also referred to as the histogram minimum method [37], was applied. This straightforward method is effective for cloud-free conditions and provides reasonable atmospheric corrections. The DP method assumes that most of the radiance detected by the satellite sensor from dark objects is due to atmospheric scattering, particularly at visible wavelengths. Pixels from dark areas were used to estimate the amount of atmospheric path radiance in the sensor data. By subtracting the atmospheric radiance from the total sensor radiance, the corrected image is adjusted to reflect the true surface properties, with the assumption that dark targets have zero surface reflectance. After preprocessing spectral bands of satellite imagery from each year, they were stacked or composited to prepare the multiband image. Then, satellite images were trimmed within the specified Area of Interest (AOI) by utilizing the masking tool in ArcGIS software.

3.2 Classification of satellite image

Masked satellite data from the mentioned years is classified using the Maximum Likelihood Classification (MLC) technique into four major land use/land cover classes: vegetation, built-up land, water bodies, and barren land. The MLC technique is preferred over other classification methods because it considers cost and probability distribution functions [38]. When classifying an unknown pixel in the MLC technique, it calculates variance and covariance, distinguishing it from other classification methods [39].

3.3 Accuracy assessment

Accuracy assessment is essential to assess the consistency of a classified image or the quality of the precise information derived from it [40, 41]. An error matrix is prepared using the 100 GCP (Ground control Points) sample collected from all four classified areas (25 for each category). That Matrix facilitates the calculation of the producer's accuracy (Eq. 3), user's accuracy (Eq. 2), overall accuracy (Eq. 1), and notably Kappa index (Eq. 4) of classified images.

These can be calculated using the following equations:

$$\text{Overall accuracy} = \frac{T_{ccp}}{T_{rp}} \times 100 \tag{1}$$

Table 1 Details of the downloaded image

Year	Satellite	Sensor	Scene_ID	No. of Bands	DOA	Spatial Resolution (m)
1990	Landsat-5	TM	LT05_L1TP_140046_19900418_20200916_02_T1	7	18-04-1990	30
2000	Landsat-7	ETM^{+}	LE07_L1TP_140046_20000421_20200918_02_T1	8	21-04-2000	30
2010	Landsat-5	TM	LT05_L1TP_140046_20100425_20161015_01_T1	7	25-04-2010	30
2020	Landsat-8	OLI/TIRS	LC08_L1TP_139046_20200328_20200822_02_T1	11	28-03-2020	30

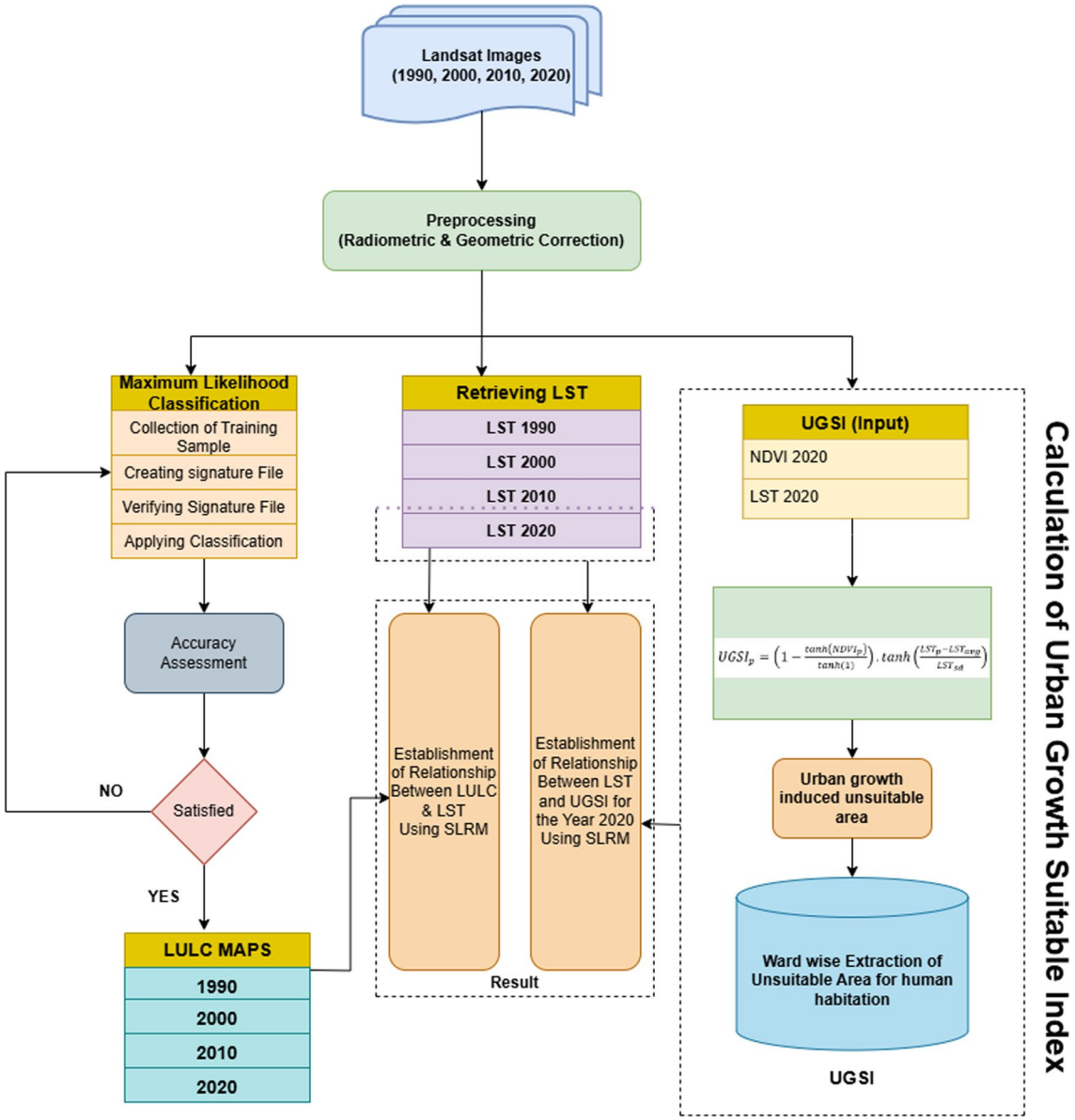

Fig. 2 Methodology Flow Chart

Here T_{ccp} is the total number of correctly classified pixels in the classified image.
And T_{rp} is the total number of reference pixels

$$\text{User Accuracy} = \frac{(T_{ccp})_i}{(T_{rp})_{i(R)}} \times 100 \tag{2}$$

Here $(T_{ccp})_i$ is the total number of correctly classified pixels of ith category of the land use.
And $(T_{rp})_{i(R)}$ is the total number of reference pixels in ith category of Land use (Row total)

$$\text{Producer Accuracy} = \frac{(T_{ccp})_i}{(T_{rp})_{i(c)}} \times 100 \tag{3}$$

And $(T_{rp})_{i(C)}$ is the total number of reference pixels in i.th category of Land use (Column total)

$$\text{Kappa Coefficient} = \frac{\left(T_{rp} \times \sum_i^n (T_{ccp})_i\right) - \left(\sum_i^n \left[(T_{rp})_{i(C)}\right] \times \sum_i^n \left[(T_{rp})_{i(R)}\right]\right)}{T_{rp}^2 - \left(\sum_i^n \left[(T_{rp})_{i(C)}\right] \times \sum_i^n \left[(T_{rp})_{i(R)}\right]\right)} \quad (4)$$

Here, 'n' is the number of categories of land use.

The range of the Kappa coefficient lies between 0 and 1. Values closer to 1 show that classified images strongly agree with ground truth data.

3.4 Population dynamics of Cuttack City

Assessing the impact of urban development on the environment, with a specific focus on the escalation of surface temperatures within city regions, is intricately linked to the dynamics of population growth. The growing urban population necessitates rapidly expanding critical infrastructures, residential structures, and transportation networks. This imperative, in turn, compels the conversion of natural landscapes into impermeable surfaces, predominantly constituted of materials such as asphalt and concrete.

To analyze the population scenario of Cuttack City, it is essential to collect population data for our study years. However, the years 1990, 2000, and 2010 are chosen for the present study. Although the census was undertaken in 1991, 2001, and 2011, this study considers the population of Cuttack City in the respective census years as the population for the study years (1990, 2000, and 2010). As the 2021 census has not yet been conducted, to calculate the population for 2020, the census data has to be interpolated.

Assuming population growth is exponential, applying the following formula (Eq. 5), the population growth rate per year is determined [42].

$$P_{(x+10)} = P_x(1+r)^{10} \quad (5)$$

Here P_x is population in census year x.

P_{x+10} is population in census year x + 10.

r is the rate of annual population growth and it is calculated using (Eq. 6).

Where,

$$r = \frac{\ln\left(\frac{P_2}{P_1}\right)}{(t_2 - t_1)} \quad (6)$$

P_1—population in time t_1.

P_2—population in time t_2.

t_1 and t_2 are in years.

To analyze the population growth pattern in Cuttack City, a quadratic distribution was chosen as the best model because of its strong correlation coefficient of 0.995, surpassing other models (Fig. 3). This quadratic model is now being employed for future population projections in Cuttack City. The formula for estimating population growth in Cuttack City using this model is as follows (Eq. 7)

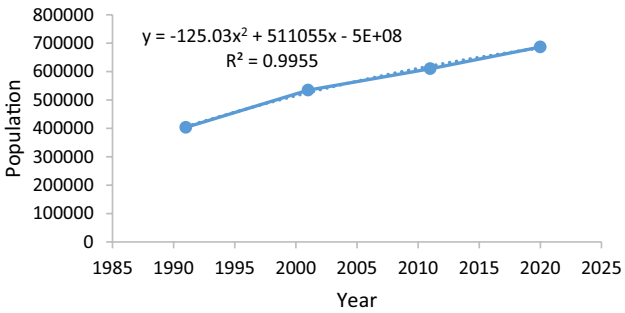

Fig. 3 Population scenario of Cuttack City

$$y = -125.03x2 + 511055x - 5E + 08 \quad (7)$$

Here, y is the population of Cuttack City, and x is the year.

3.5 Retrieving LST

Band-6 of Landsat-5 (TM), Landsat-7 ETM+, and band-10 Landsat-8(OLI/TIRS) were used to retrieve LST for Cuttack City. At first, Landsat images' spectral radiance of thermal infrared bands is converted into a sensor brightness temperature using Planck's equation (Eq. 8).

$$BT = \frac{C_2}{\left(\lambda_i * \ln\left(1 + \frac{C_1}{L_i \lambda_i^5}\right)\right)} \quad (8)$$

Here, BT is brightness temperature in °K. C_1 and C_2 are constants, $C_1 = 1.19104356 \times 10^{-16}$ W.m^2, $C_2 = 1.4387685 \times 10^4$ µm K, λ is emitted radiance wavelength for peak response (λ = 11.5 µm for Landsat band-6 data, 10.9 µm for band 10 and 12 µm for band 11 of Landsat-8 satellite data) [43].

Planck's law calculates the brightness temperature from the top of the atmospheric radiation. Top of atmospheric radiance results from a combination of radiance emitted by the Earth's surface, upward radiance from the atmosphere, and radiance from the sky in a downward direction [44]. Therefore, reflected irradiance from surface absorption upward emission needs to be corrected to find the exact LST [45, 46]. Land surface emissivity is calculated to correct the TOA radiance.

The emissivity of a surface is governed by many environmental components like its chemical composition, geometrical structure, water content roughness, etc. [43]. In vegetative areas, emissivity varies with plant species' variation and canopy densities. A close correlation exists between land surface emissivity and the Normalized Difference Vegetation Index (NDVI). Hence, emissivity is found in NDVI, shown in Table 2.

The NDVI is used to find vegetation coverage of Cuttack City. NDVI index value rests on vegetation coverage and the physiological state of vegetation [47, 48].

NDVI given by formula (Eq. 9),

$$NDVI = \frac{NIR - RED}{NIR + RED} \quad (9)$$

Here NIR—Near Infrared band.
RED—Red Band.

3.6 Calculating LST

LST corrected from land surface emissivity is assessed using Eq. 10 below [46–48].

$$LST = \frac{B_T}{1 + \left(\lambda * \frac{B_T}{\rho}\right) * \mathrm{Ln}(\varepsilon)} \quad (10)$$

Here,
LST—Land surface temperature,

Table 2 Range of NDVI and its corresponding Spectral emissivity value of land surface

NDVI	Land surface emissivity
NDVI < -0.185	0.995
− 0.185 < = NDVI < 0.157	0.97
0.157 < = NDVI < = 0.727	1.0094 + 0.047 ln (NDVI)
NDVI > 0.727	0.99

BT—at sensor Brightness Temperature in °K,
λ—Wavelength of emitted radiance,
ρ = 0.01438 mk, and ε- land surface emissivity.

3.7 Determination of urban growth suitability index (UGSI)

Understanding and managing urban environmental concerns depend on identifying and measuring Suitable and unsuitable or underprivileged areas inside a city. The health and well-being of locals may be significantly impacted by these unsuitable environments, which are frequently characterized by high surface temperatures and a lack of green space. UGSI is an index derived from finding suitable and unsuitable areas of the city in which to live [49]. The UGSI is calculated using the formula (Eq. 11)

$$UGSI_p = \left(1 - \frac{tanh\left(NDVI_p\right)}{tanh(1)}\right).tanh\left(\frac{LST_p - LST_{avg}}{LST_{sd}}\right) \tag{11}$$

Here, $UGSI_p$ is the Urban Growth Suitability Index of pixel p.
$NDVI_p$—NDVI of pixel p.
LST_p—LST of pixel p.
LST_{avg}—Average LST value of all pixels in the image.
LST_{sd}—Standard deviation of LST value of all pixels in the image.

Areas with high NDVI and less LST value have a low UGSI compared to areas with low NDVI and high LST value. Hence, this index will help identify suitable and unsuitable areas to live. Here, the hyperbolic tangent function is used so that for non-negative NDVI values, UGSI will be between − 1 and + 1 [50]. In this study, UGSI was reclassified into 4 different classes, namely, Suitable area (− 1 to − 0.5), moderately suitable (− 0.5–0), unsuitable area (0–0.5) and highly unsuitable area (0.5–1.0) (Table 3).

4 Result

4.1 Land use/land cover change

The classified satellite images of the study area for 1990, 2000, 2010, and 2020 underwent an accuracy assessment to evaluate the reliability of the land cover classifications. Overall accuracy of classification results was above 93% for all the studied periods (Table 4). The Kappa coefficient value for the studied year shows strong agreement between classified and ground truth data.

The analysis of the classified imagery has unveiled substantial transformations within the study area over the four studied periods (Figs. 4, 5, 6, 7). Noteworthy is the remarkable expansion of built-up land, which substantially increased from 33.68 km^2 (41.31%) in 1990 to 39.38 km^2 (48.31%) in 2000. This trend rose to 41.30 km^2 (50.66%) in 2010, reaching 53.28 km^2 (65.35%) by 2020. This urbanization phenomenon encompasses both planned and unplanned developments. Notably, many of the newly established built-up land in 2020 are situated within previously vegetated zones and water bodies within Cuttack City. In contrast, the extent of vegetation has exhibited a declining trend, diminishing from 34.19 km^2 (41.94%) in 1990 to 28.16 km^2 (34.55%) in 2000, further reducing to 18.90 km^2 (23.18%) in 2010, and reaching 16.62 km^2 (20.39%) by 2020. Simultaneously, barren Land has witnessed an increase from 3.48 km^2 (4.27%) in 1990 to 10.2 km^2 (12.51%) in 2000 and 17.10 km^2 (20.98%) in 2010, subsequently decreasing to 9.08 km^2 (11.14%) in 2020. Additionally, water bodies have experienced a decline from 10.17 km^2 (12.47%) in

Table 3 UGSI Range

UGSI classes	Range
Suitable	− 1 to − 0.5
Moderately Suitable	− 0.5 to 0
Unsuitable	0 to 0.5
Highly Unsuitable	0.5 to 1.0

Table 4 Accuracy assessment

Sl. no	Accuracy	LULC	Cuttack city			
			1990 (%)	2000 (%)	2010 (%)	2020 (%)
1	Producer accuracy	Built-up Land	90	94	93	94
		Vegetation	86	85	89	85
		Water bodies	93	92	92	94
		Barren Land	88	91	91	93
2	User accuracy	Built-up Land	93	88	87	91
		Vegetation	92	93	93	94
		Water bodies	89	89	91	93
		Barren Land	94	92	89	92
3	Overall accuracy		93.15	93.12	93.02	93.25
4	Kappa Coefficient		0.92	0.90	0.89	0.93

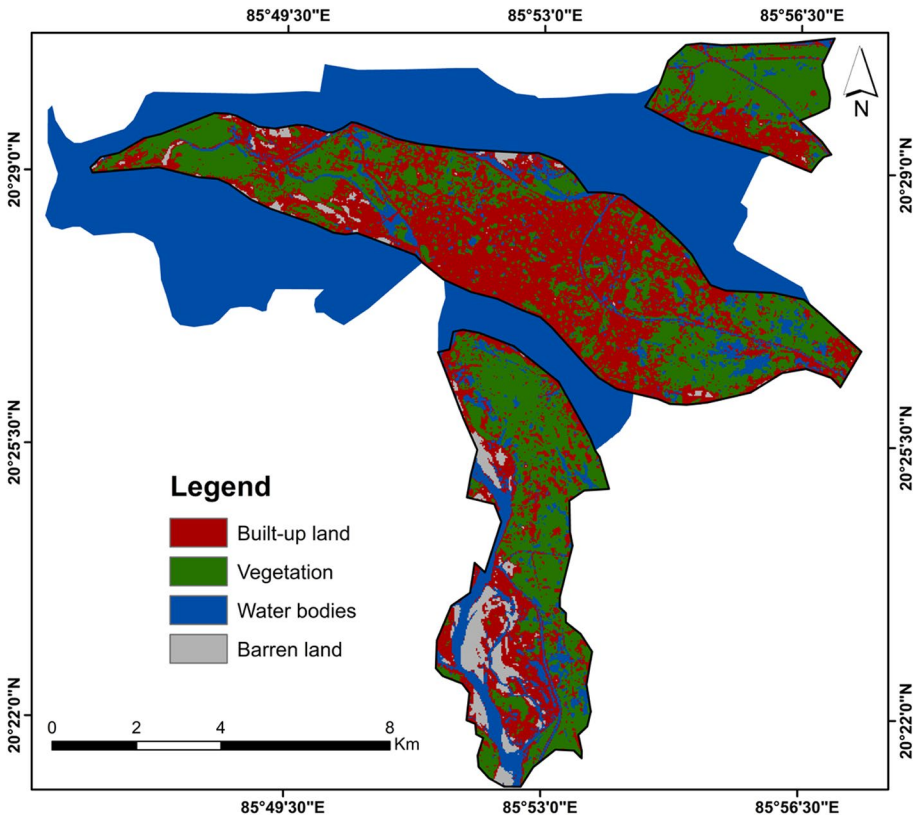

Fig. 4 LULC 1990

1990 to 3.777 km^2 (4.63%) in 2000 and 4.21 km^2 (5.16%) in 2010, with a further reduction to 2.54 km^2 (3.11%) in 2020 (Table 5). This comprehensive transformation, as evidenced by land use changes, underscores the dynamic interplay between urbanization, vegetation loss, and alterations in natural land features within Cuttack City.

This LULC change in Cuttack City is attributed to the developmental work of the Odisha Government during the late 90's. The Cuttack Development Authority (CDA) developed many planned housing schemes on the western side of Cuttack City. Simultaneously, the Government of Odisha initiated a vigorous push for infrastructural development within the city. This impetus led to the emergence of malls, hotels, multiplexes, single-brand retail outlets, and educational institutions in and around the city. These developmental actions catalyzed the city's economic growth, subsequently attracting people from various districts of Odisha in pursuit of improved employment opportunities, education, healthcare, and other amenities. This population influx into the city also witnessed the proliferation of slum settlements, unplanned road networks, unhygienic conditions, a decrease in the city's green space, and a rise in city temperature.

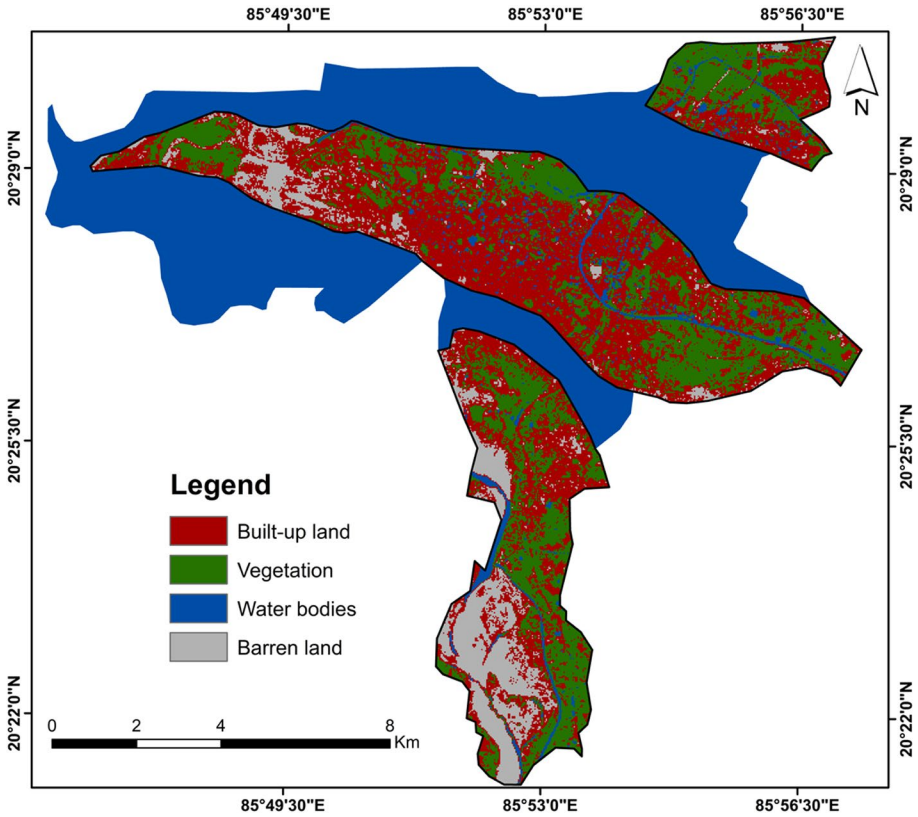

Fig. 5 LULC 2000

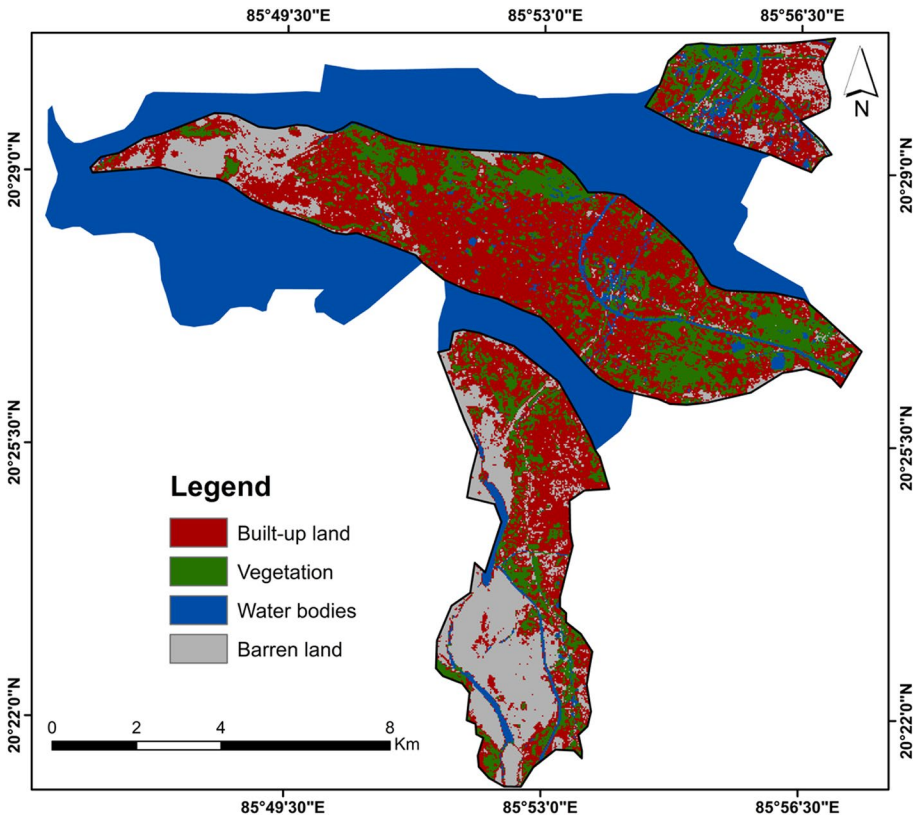

Fig. 6 LULC 2010

Fig. 7 LULC 2020

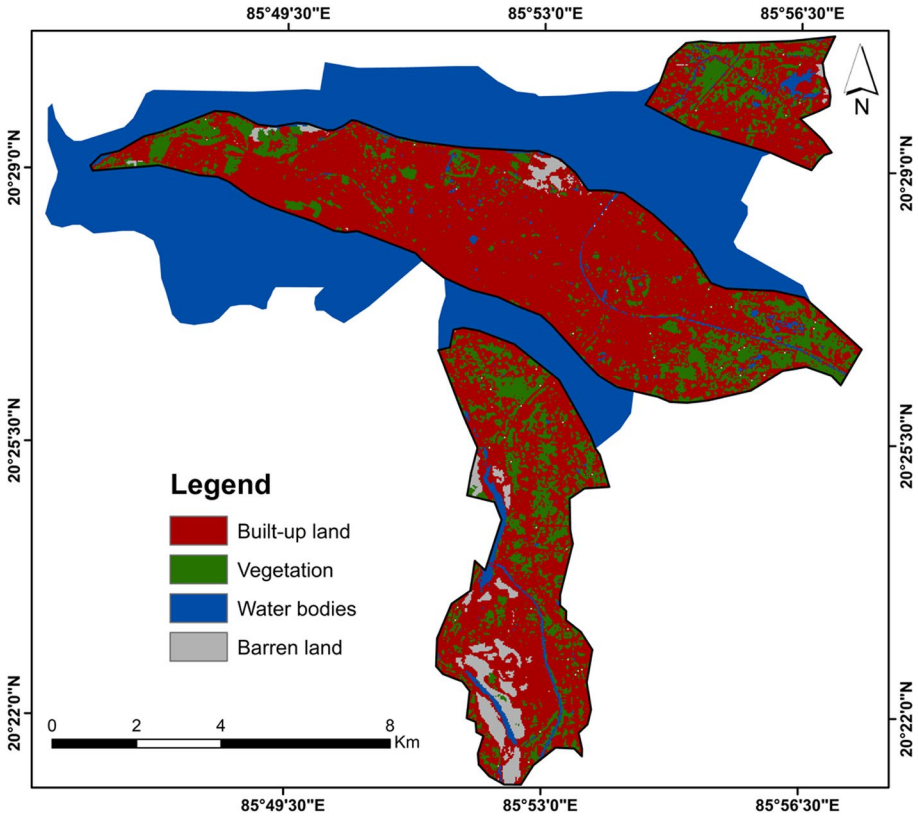

Table 5 Area Statistics

Year	Landuse/land cover							
	Built-up land		Vegetation		Water bodies		Barren land	
	Area(km^2)	Percentage	Area (km^2)	Percentage	Area (km^2)	Percentage	Area (km^2)	Percentage
1990	33.68	41.32	34.19	41.94	10.17	12.48	3.48	4.27
2000	39.38	48.31	28.16	34.55	3.777	4.63	10.2	12.51
2010	41.3	50.67	18.9	23.19	4.21	5.16	17.1	20.98
2020	53.28	65.36	16.62	20.39	2.54	3.12	9.08	11.14

4.2 Population and built-up land relationship

The demographic scenario of Cuttack City, as illustrated over the years 1990, 2000, 2010, and 2020, reveals a dynamic relationship between urban expansion and population growth. The built-up land has experienced a substantial increase, corresponding to the rising population. From 1990 to 2020, the built-up land has expanded by 19.60 km^2, reflecting a 58.19% increase (Table 6). This constructive relationship underscores the profound impact of population growth on urban development and the demand for residential and commercial spaces [51]. As the population surged from 4,03,418 in 1990 to 6,86,627 in 2020, the absolute increase of 283,209 people further fueled the need for expanded built-up land to accommodate the rising population. The simultaneous rise in the population and the number of the built-up regions highlights the delicate relationship between demographic trends and urbanization. This underscores the need for smart urban planning to guarantee sustainable and well-managed city development amidst ongoing population expansion. The built-up area and population growth over the years are displayed in Fig. 8.

Table 6 Urban built-up land area statistics of Cuttack City

Year	Built-up Land	Growth in built-up land	Percentage growth in built-up land	Population	Absolute growth in population	Percentage increase in population
1990	33.68	–	–	403,418	–	–
2000	39.38	5.70	7.00	534654	131236	32.53
2010	41.30	1.92	2.35	610189	75535	14.13
2020	53.28	11.98	14.70	686627	76438	12.53
	–	19.60	58.19	–	283209	70.20

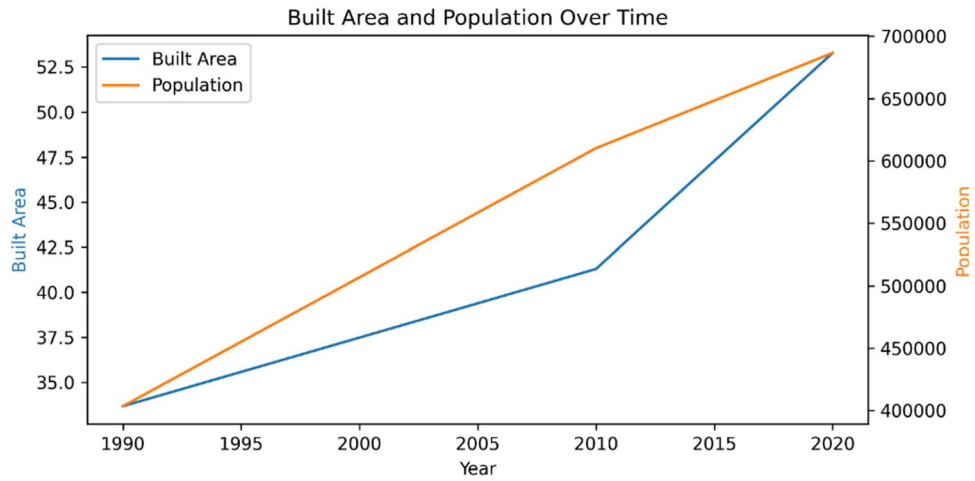

Fig. 8 Trend of Population and Built-up Area of Cuttack City

Table 7 Temporal Variation of Temperature

Year	LST		
	Maximum	Minimum	Mean
1990	32.07	23.22	26.92
2000	33.89	26.07	29.72
2010	36.91	27.08	32.08
2020	38.67	29.15	33.45

4.3 Retrieval of LST

Over the years, Cuttack City's temperature variation has revealed intriguing patterns and trends. From 1990 to 2020, there was a noticeable upward trajectory in both maximum and minimum temperatures (Table 7). The maximum temperature has consistently risen, starting at 32.07 °C in 1990 and reaching 38.67 °C in 2020. Similarly, the minimum temperature has experienced an upward trend, starting from 23.22 °C in 1990 to 29.15 °C in 2020. Over the observed years, the mean LST has revealed a discernible rise, starting from 26.92 °C in 1990 and ascending to 33.45 °C in 2020. This means that temperature trends affect the city's climate and potentially impact various aspects of urban life. The rising mean temperature could influence the duration and intensity of heat waves, affecting the health and well-being of the city's inhabitants. Additionally, it may contribute to shifts in precipitation patterns.

The dynamic shift or temperature variation over the 30 years is spatially mapped to show temperature changes manifest across different locations within the city (Figs. 9, 10, 11, and 12). In 1990, the Central area of the town showed higher temperatures than the corner areas because of less urban growth, but in due course of time, with rapid growth in built-up land, city temperature rises that can be seen in 2020 when most of the city shows higher temperature.

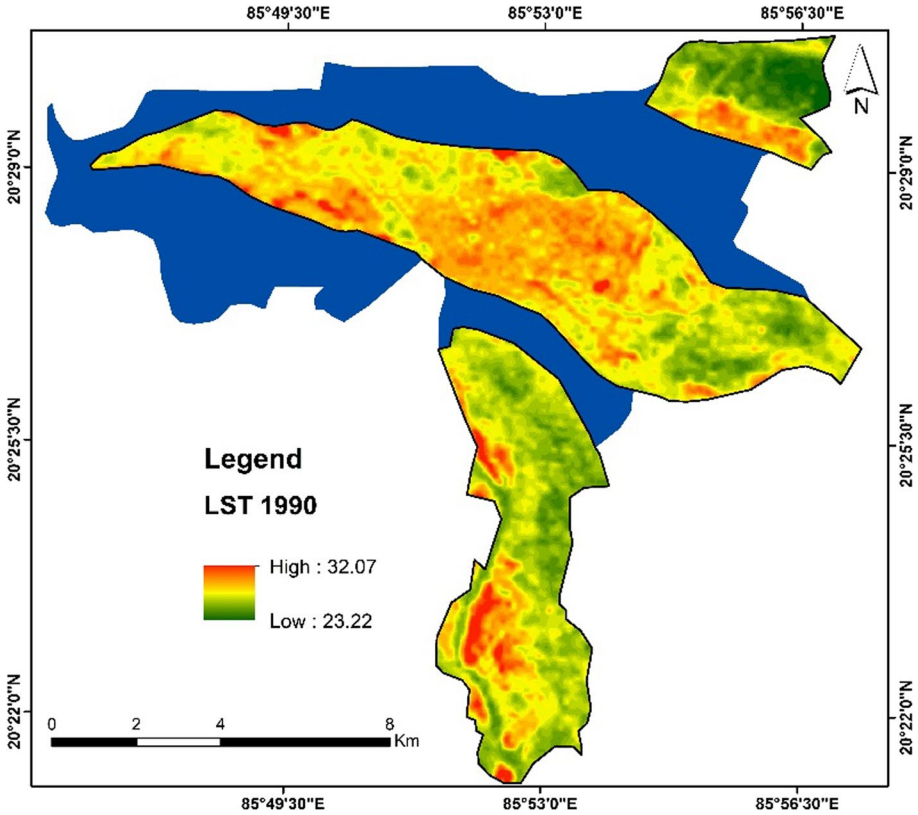

Fig. 9 LST 1990

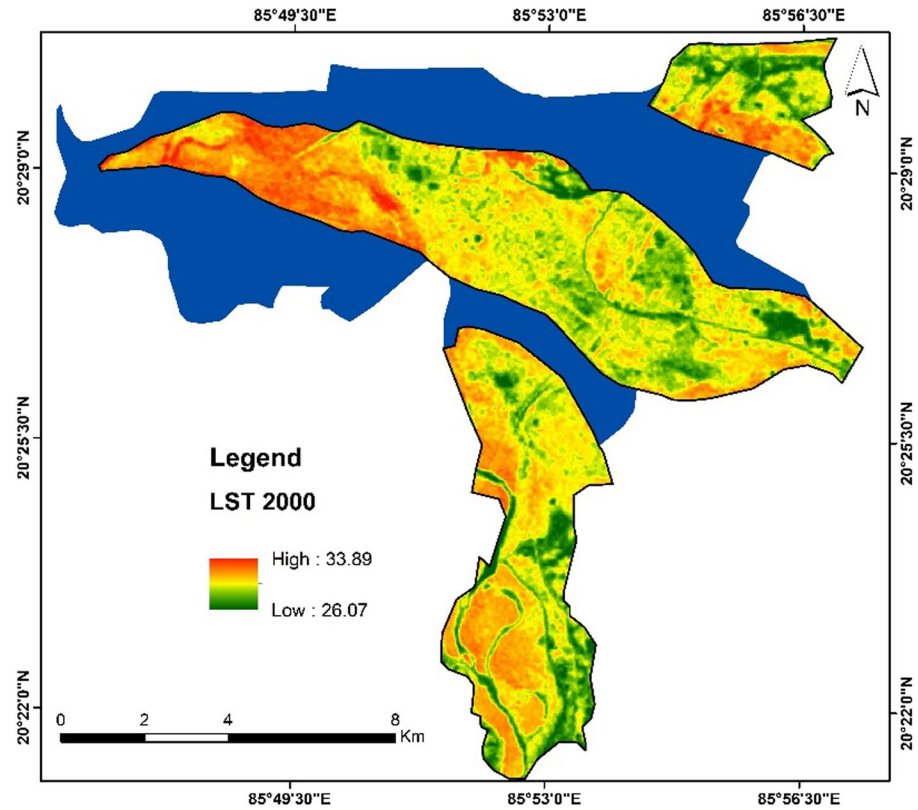

Fig. 10 LST 2000

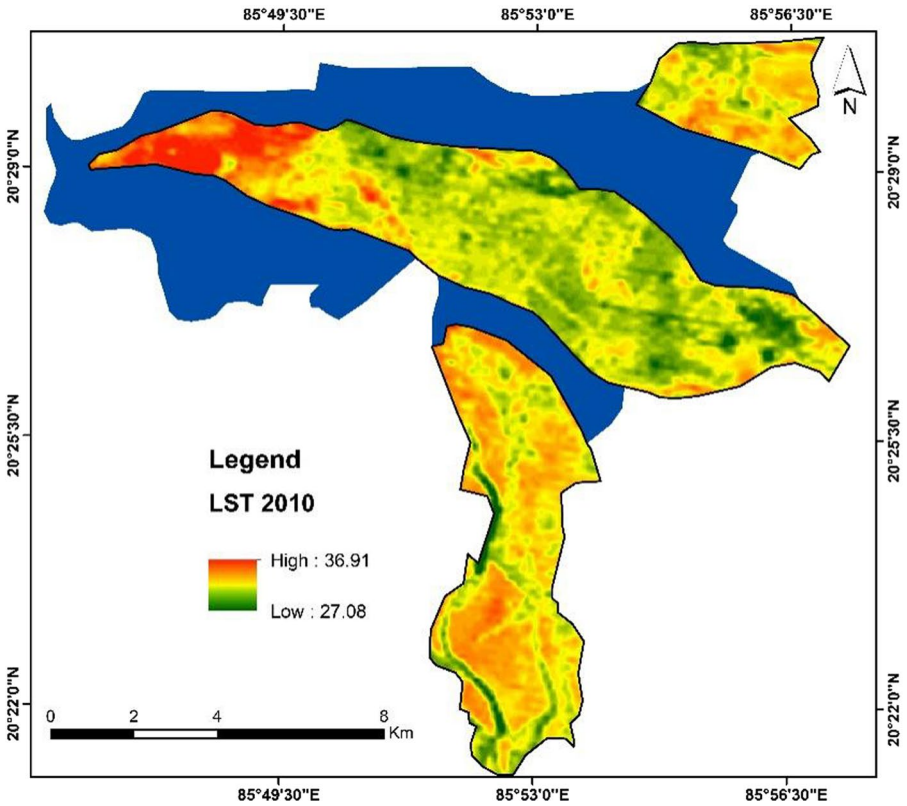

Fig. 11 LST 2010

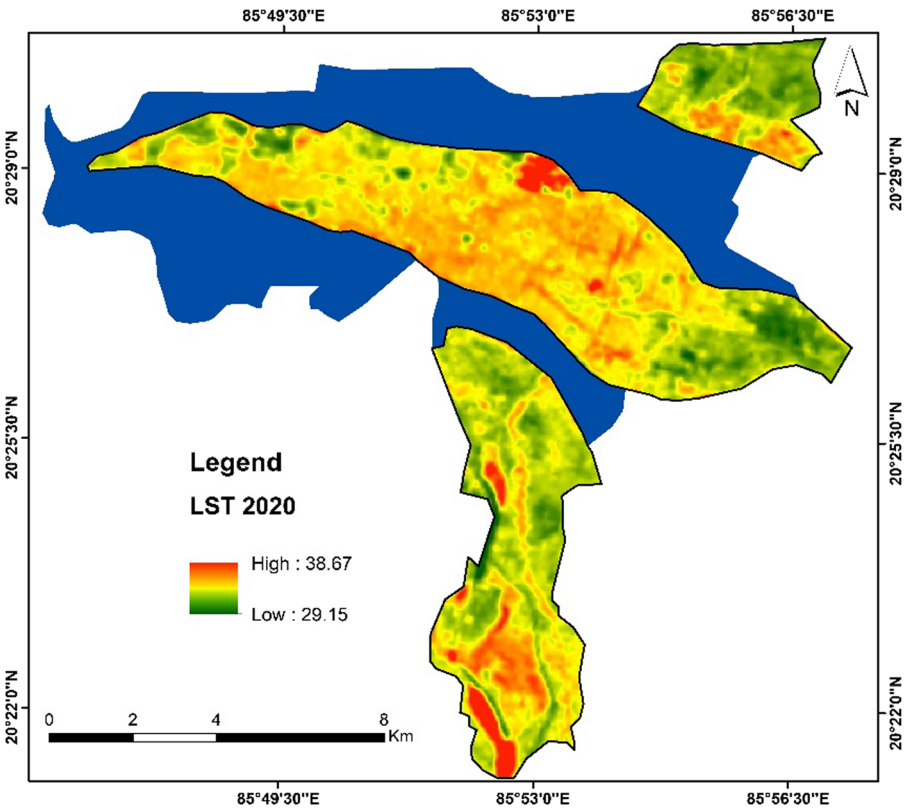

Fig. 12 LST 2020

4.4 Relationship between LULC and LST

4.4.1 Establishment of relationship with graphical comparison

Various techniques and models were employed to investigate the correlation between LST and the different LULC types [52]. Figure 13 portrays the dynamic changes in the area distribution of various LULC categories over 30 years with fluctuations in mean LST. The graph representing the relationship between Vegetation and Mean LST reveals a negative correlation. This suggests that as the proportion of vegetation decreases, LST tends to increase. In essence, it indicates that vegetation plays a crucial role in cooling the urban environment, but its coverage has significantly diminished over three decades.

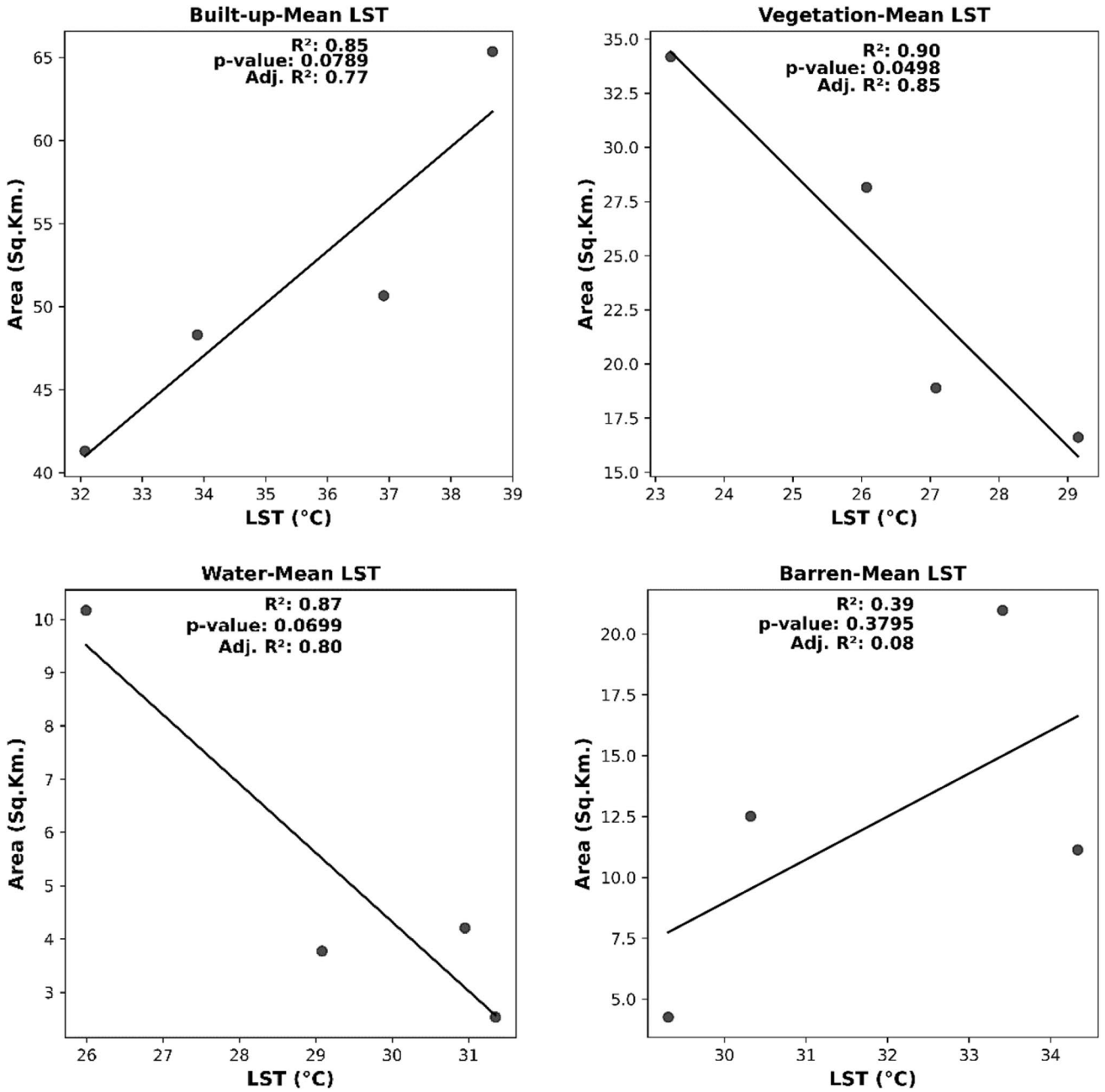

Fig. 13 Mean LST and LULC Variation

Similarly, the Built-up land shows a positive correlation with LST; in the study period, the built-up land increased from 33.68 km^2 in 1990 to 53.28 km^2 in 2020, contributing to the sharp rise in City temperature. Waterbodies that once had a 12.47% share of the city's total land mass shrunk to only 3.11% in 2020. The relationship graph between Mean LST and Waterbodies shows a negative slope that shows a decrease in the area of waterbodies in the city, contributing to the rise in urban temperature. Barren Land also shows a somewhat positive relationship with LST. Over our study year, the area of barren Land fluctuates in a zigzag manner, leading to a rise in LST. The graph between Mean LST and the area of barren Land also shows a positive slope, suggesting that barren Land has a positive correlation with LST.

4.4.2 Establishment of relationship with simple linear regression model

A simple linear regression model can establish the relationship between LULC and LST. The model Summary is shown in Table 8. In this model, LULC serves as the independent variable, while LST is the dependent variable

$$LST = 29.18 + 0.22 * (LC)_{Built-Up} \quad (12)$$

$$LST = 32.80 - 0.67 * (LC)_{Water} \quad (13)$$

$$LST = 33.39 - 0.29 * (LC)_{Vegetation} \quad (14)$$

$$LST = 21.50 + 0.27 * (LC)_{Barren} \quad (15)$$

In the regression equation (Eq. 12), where $LC_{Built-up}$ represents the independent variable 'Built-up land,' with a constant value of 29.18 and a coefficient of 0.22, the positive coefficient indicates a positive relationship between LST and Built-up land. The results suggest a statistically significant and relatively strong linear relationship between LST and the Built-up land, with an R-squared value of 0.8483, indicating that approximately 84.83% of the variability in LST can be explained by changes in the Built-Up land.

In Eq. 13, LC_{Water} is the independent variable representing water bodies, and the dependent variable is LST. A strong negative linear relationship exists between LST and the Water Cover in the area. The negative coefficient of -0.67 indicates that as the proportion of water cover increases, LST tends to decrease. The high correlation coefficient ($R = -0.66$) further confirms the strength of this negative relationship, with a coefficient of determination (R-squared) of 0.86, indicating that approximately 86% of the variability in LST can be explained by changes in the Waterbodies area.

In (Eq. 14), $LC_{Vegetation}$ is Vegetation cover, the independent variable. A moderate negative linear relationship exists between LST and the proportion of Vegetation Cover in the area. The negative coefficient of – 0.29 suggests that as the proportion of vegetation cover increases, LST tends to decrease. The correlation coefficient ($R \approx -0.286$) indicates the strength of this negative relationship, while the coefficient of determination (R-squared) of 0.902 implies that approximately 90.2% of the variability in LST can be explained by changes in Vegetation area.

In (Eq. 15), LC_{Barren} is the Independent variable representing Barren Land. The relationship between LST and the proportion of Barren Land area is positive but relatively weak. The positive coefficient of 0.27 indicates that as the proportion of barren land cover increases, LST tends to increase, though the effect is not very strong. The correlation coefficient ($R = 0.217$) suggests a positive but modest relationship. The R-squared value of 0.39 indicates that changes in Barren land area can explain approximately 39% of the variability in LST.

Given the coefficients' high significance levels (low p-values), strong R-squared values, and satisfactory standard errors, this regression model can be considered valid. The models for Vegetation and Water, in particular, demonstrate robust

Table 8 Model summary

LULC	Regression coefficient (R)	R-Squared	Standard error	p-Value
Built-up land	0.27	0.85	4.2	0.03
Vegetation	– 0.286	0.902	1.692	0.002
Water bodies	– 0.66	0.86	1.11	0.001
Barren land	0.217	0.39	2.67	0.008

relationships with LST, supported by their extremely low p-values and low standard errors. The Built-up land model is also significant, though it has a slightly higher standard error. The Barren Land model, while relatively weaker, still provides valuable insights. Overall, these findings highlight the model's validity and reliability in explaining the influence of LULC categories on LST in the study area.

4.5 Urban growth suitability index of the Cuttack City

The UGSI is calculated using Eq. 11. Where UGSI values span from − 1 to + 1. Values close to + 1 indicate unsuitable living conditions for urban residents, while values nearing -1 denote relatively more suitable areas for urban dwellers [50]. An analysis of the UGSI results, presented in Fig. 15, reveals that the central and western regions of the city, along with select areas in the northern and southern parts, exhibit unsuitable conditions for urban living. The unsuitable living conditions in these areas can be attributed to the lack of vegetation and extensive urban development. The densely built-up areas contribute to an environment that may not be conducive to a high quality of life, thus making them unsuitable for urban habitation.

4.5.1 Relationship between LST and UGSI

To establish the relationship between UGSI and a variation of LST for different land uses and land cover SLRM is used. Here, LST is taken as the independent variable for this model, and UGSI is the dependent variable (Fig. 14). Results of this model are given below.

$$\mathrm{UGSI} = -5.63 + 0.19 * \mathrm{LST}_{\mathrm{Vegetation}} \tag{16}$$

$$\mathrm{UGSI} = -7.40 + 0.24 * \mathrm{LST}_{\mathrm{Waterbodies}} \tag{17}$$

$$\mathrm{UGSI} = -4.14 + 0.14 * \mathrm{LST}_{\mathrm{Built-Up}} \tag{18}$$

$$\mathrm{UGSI} = 0.78 + 0.00 * \mathrm{LST}_{\mathrm{Barren}} \tag{19}$$

In Eq. 16, $\mathrm{LST}_{\mathrm{Vegetation}}$ is an independent variable representing the value of LST in the Vegetation area for the year 2020. The results of the analysis reveal a highly significant and strong relationship between LST and the UGSI within the vegetative area of the city. An increase in LST is associated with an increase in UGSI, and the regression model can explain approximately 77.95% of the variation in UGSI based on variations in LST within the vegetation category.

In (Eq. 17), $\mathrm{LST}_{\mathrm{Waterbodies}}$ is an independent variable representing the value of LST in Waterbodies for 2020. The model result shows that waterbodies exhibit a highly significant and strong relationship between LST and the UGSI, with a very low p-value (0.0000) and an elevated R-squared value (0.8557), indicating the robust explanatory power of LST for UGSI. The regression equation reveals that as LST increases, UGSI also rises for waterbodies.

In (Eq. 18), $\mathrm{LST}_{\mathrm{Built\text{-}Up}}$ is an independent variable. The analysis within the 'Built-up' land use category reveals a highly significant relationship between LST and the UGSI, characterized by a low p-value (0.0000) and substantial explanatory power (R-squared: 0.6705). The regression equation indicates that an increase in LST is associated with a corresponding rise in UGSI, highlighting the adverse impact of higher temperatures on living conditions within the city's built-up areas.

In (Eq. 19), $\mathrm{LST}_{\mathrm{Barren}}$ is an independent variable. In the "Barren" land use category, a significant relationship is observed between LST and the UGSI. The findings include a moderately low p-value (0.0442) and a notable R-squared value (0.6773). The regression equation shows that, in this context, UGSI remains relatively stable (0.00 change) as LST varies, indicating a limited influence of temperature on living conditions within barren areas.

5 Discussion

The study reveals the critical role that LULC plays in moderating LST. As urban areas expand and vegetation cover diminishes, the amount of impervious surfaces, such as buildings and roads, increases, leading to greater heat absorption and reduced cooling through evapotranspiration. The loss of green spaces has had detrimental effects on local microclimates,

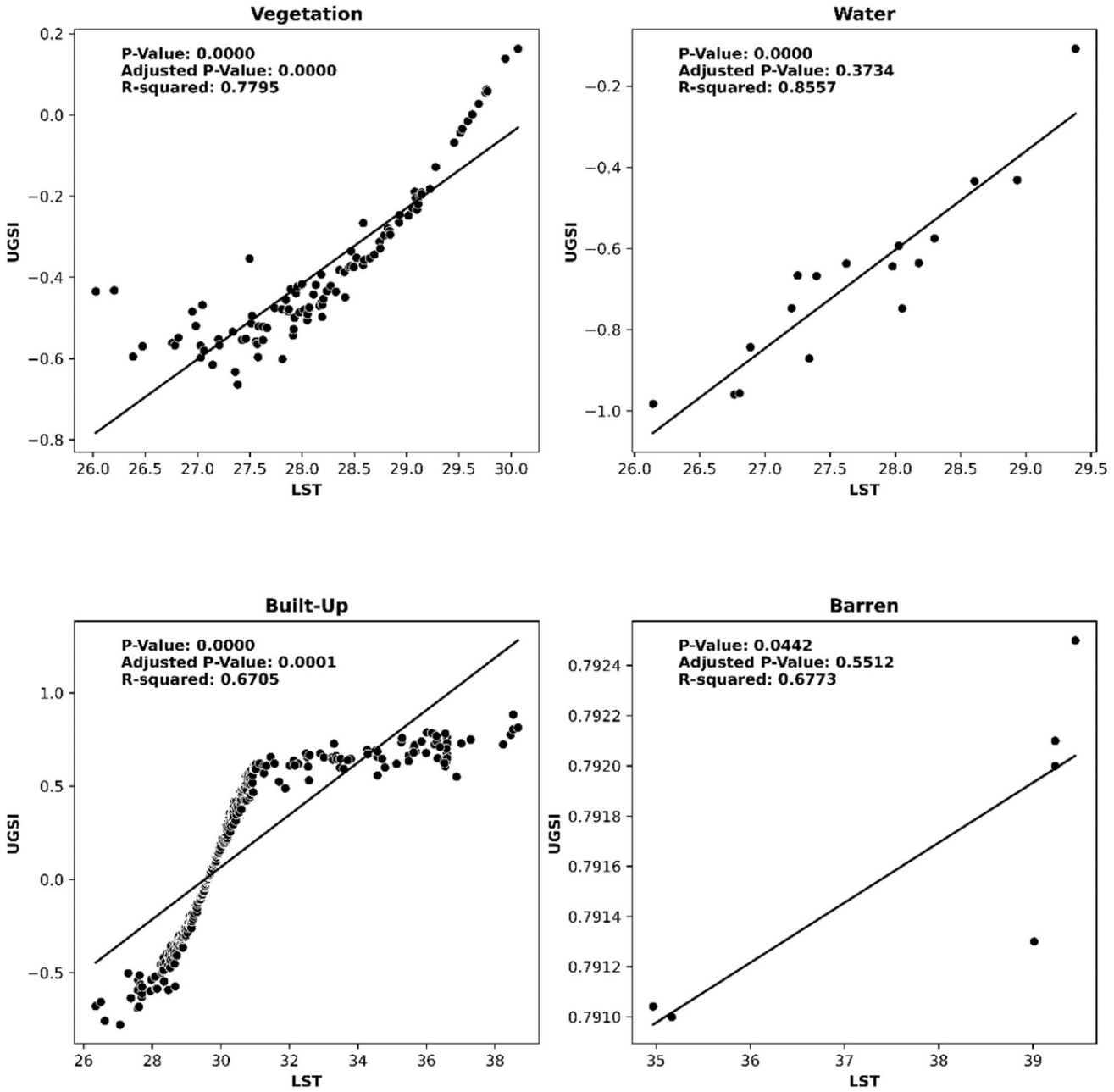

Fig. 14 Variation of UGSI with LST for different LULC categories

leading to the intensification of the UHI phenomenon. These findings are consistent with research from Sialkot, Pakistan, where the transformation of green spaces into built-up land resulted in a noticeable increase in LST and a growing urban heat island effect [53]. Similarly, in Portugal, the conversion of green and water areas into urban infrastructure between 1990 and 2018 contributed to rising temperatures in coastal regions, reinforcing the importance of maintaining green spaces to mitigate heat [54].

A key finding of this study is the identification of heat vulnerability zones across Cuttack City. Among the 59 administrative wards in the city, 27 were found to be particularly susceptible to high temperatures, largely due to sparse vegetation and high levels of built infrastructure (Fig. 15). These areas cover approximately 19.61% of the city, indicating regions where the urban heat effect is most severe and where urgent intervention is needed. This mirrors the findings from Addis Ababa, where the rapid expansion of built-up land and the decrease in urban green spaces were found to contribute significantly to increased LST, with areas of high built-up density experiencing the highest temperatures [55].

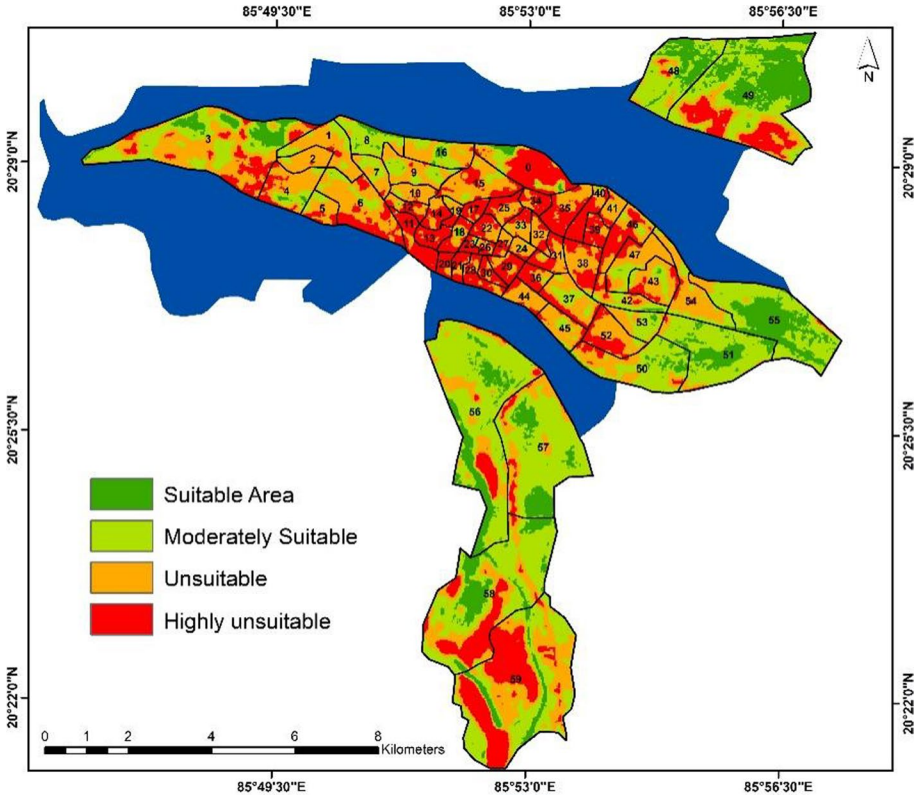

Fig. 15 Suitable and unsuitable area Superimposed with Ward Boundary

In contrast, only 13.21% of the city was deemed suitable for habitation, characterized by more favorable conditions of green cover and lower LST. This study highlights that the urban sprawl in Cuttack City is contributing to an environmental imbalance, where the urban core is significantly warmer than the surrounding peri-urban areas. As cities grow, these extreme heat zones may become increasingly inhospitable for residents, exacerbating health risks associated with high temperatures, such as heat stroke and respiratory illnesses. Similar concerns were raised in the Leiria region of Portugal, where the rapid increase in built-up land from 1990 to 2018 contributed to a rise in LST, directly affecting the livability of urban areas [54]. These findings are also echoed in Sialkot, where an increase in built-up land led to a significant rise in LST, directly impacting the local population's exposure to extreme heat [53].

The Urban Growth Suitability Index, used in this study, offers a valuable tool for identifying areas within Cuttack City that are most vulnerable to heat, thereby aiding in urban planning decisions. The UGSI results indicate that densely populated regions of Cuttack City, such as Badambadi, Odia Bazar, Mangala Bag, Bauxi Bazar, Mahanadi Vihar, and CDA Sectors 6, 7, 10, and 11, are classified as unfavorable for residents (Fig. 16). Specifically, ward numbers 4, 5, 6, 11, 12, 13, 14, 17, 18, 20, 21, 22, 23, 25, 26, 27, 28, 29, 30, 34, 35, 37, 39, 40, 46, 52, and 59 (Fig. 17) of the Cuttack Municipal Corporation are experiencing elevated temperatures and exhibit high UGSI values. These areas are notable for hosting key destinations, including SCB Medical College and Hospital, Ravenshaw University, National Law University, Malgodown, Barabati Stadium, and several shopping malls and market areas, these areas have huge economic potential for small and marginal businesses often leading to the development of slums in their vicinity. The southern part of the city, particularly Pratap Nagari, which is densely populated and, the northern area, the Jagatpur industrial zone of the Cuttack city identified as highly unsuitable regions, characterized by elevated LST values.

The findings underscore the need for sustainable urban development strategies, including the restoration of green spaces, better management of urban growth, and the implementation of cooling measures such as urban forests or green rooftops. Urban planners and policymakers should prioritize the development of targeted green corridors connecting key heat-vulnerable zones such as Badambadi, Odia Bazar, and Mangala Bag with areas of higher green cover, enhancing cooling effects and improving urban livability. In densely populated wards with high UGSI values, urban redevelopment initiatives should include mandating green rooftops, vertical gardens, and permeable pavements to reduce heat absorption. Industrial zones like Jagatpur require focused interventions, such as establishing buffer zones with dense vegetation and enforcing stricter environmental regulations to limit heat emissions. Additionally, promoting community-driven afforestation programs in peri-urban areas and implementing urban wetland restoration projects can enhance the city's

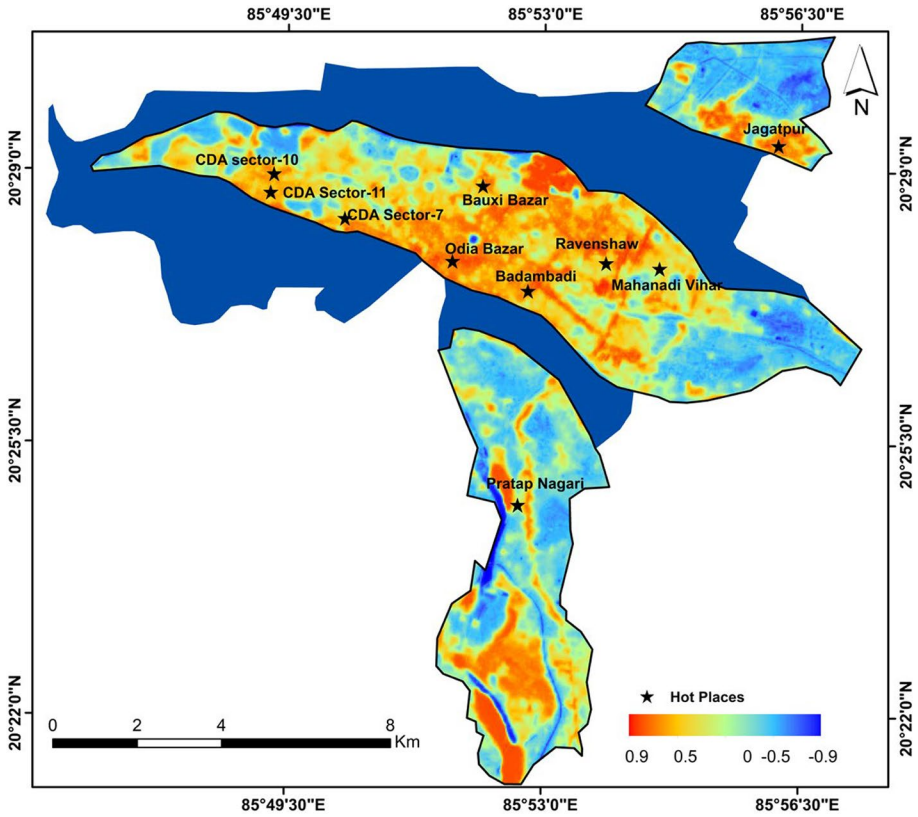

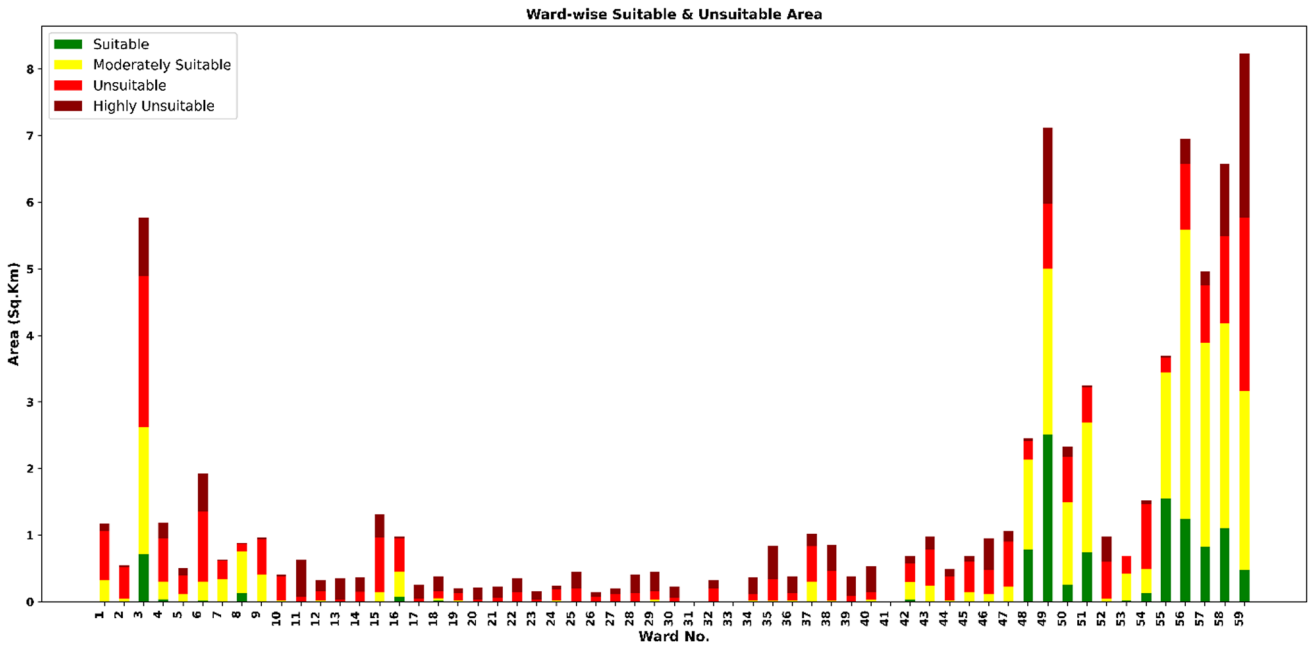

Fig. 16 Densely populated areas of Cuttack City experiencing high UGSI values

Fig. 17 Ward-wise distribution of suitable and unsuitable areas of Cuttack City

resilience against rising temperatures. These localized, actionable strategies can transform UGSI findings into effective tools for sustainable urban planning and climate adaptation in Cuttack City. These strategies have been suggested in studies across multiple cities. For instance, in Jimma, Ethiopia, GIS-based evaluations have been used to identify suitable sites for green space development, with urban green spaces recognized as crucial for enhancing urban resilience and mitigating the UHI effect [56]. Similarly, studies from Tiruchirappalli, India, emphasized the need to incorporate green

spaces into urban development to mitigate rising LST and promote climate adaptation [57]. Similarly, studies in Indore, India [58], and Sikar, India [59], also highlight the importance of green spaces in managing urban thermal environments. In Indore, the study used Cellular Automata modeling to project urban growth and found that the expansion of built-up land would continue to contribute to temperature increases. However, it also showed that the overall LST was decreasing between 2010 and 2020 due to the cool heat island phenomenon observed in surrounding rural areas.

The findings of this study contribute significantly to sustainable urban planning and climate resilience by emphasizing the critical role of green spaces and balanced urban growth in mitigating rising LST and the UHI effect [60–63]. By identifying heat vulnerability zones and mapping areas with sparse vegetation and high levels of impervious surfaces, the research provides actionable insights for integrating cooling measures such as urban forests, green rooftops, and water bodies into city planning. Overall, the research offers a framework for data-driven decision-making to guide sustainable urban development, ensuring livable and resilient environments amid rapid urbanization and climate change.

6 Limitation

While this study provides valuable insights into the relationship between LULC changes and LST in Cuttack City, there are a few limitations to consider. The spatial resolution of the satellite images used in this study may not capture minor variations in temperature and vegetation. Higher-resolution data could provide a more detailed insight into heat vulnerability and green areas. This study did not consider other factors, such as air pollution, socioeconomic conditions, or demographics, which also affect how people experience heat. Future studies that include these factors could give a more complete picture of heat vulnerability.

7 Conclusion

The increasing urban temperature due to urbanization poses a significant concern for urban planners and policymakers, as it is a primary driver of severe health issues for urban residents. Studies on LST and the environment offer crucial insights for environmental scientists assessing the impacts of urbanization. This 30-year study from 1990 to 2020 in Cuttack City reveals profound insights into the complex dynamics of LULC changes, LST variations, and identifying unsuitable areas using the UGSI. The analysis underscores a substantial transformation in the urban landscape, marked by a noteworthy expansion of the built-up regions, simultaneous declines in vegetation, and alterations in barren Land and water bodies, reflecting the escalating urbanization trends within the city. The application of Simple Linear Regression Models (SLRM) to establish relationships between LULC and LST, as well as LST and UGSI, deepens our understanding of how Land use changes influence surface temperatures. The positive correlation between built-up land and increased LST emphasizes the UHI effect, highlighting the necessity for sustainable urban planning to mitigate temperature extremes. A significant finding lies in identifying unsuitable areas within the city in 2020 using the UGSI, which incorporates both LST and NDVI. This knowledge is indispensable for directing targeted interventions in areas that require early attention. This study also advances our understanding of the UH) effect in medium-sized Indian cities by revealing how rapid urbanization, characterized by the expansion of built-up land and the decline of vegetation and water bodies, intensifies surface temperatures over time. This study is critical from an urban sustainability planning perspective in constructing future development strategies. This finding makes it clear that it is imperative to incorporate sustainability concepts into urban growth processes where environmental, social and economic features are equalized into a balanced scenario. The ways to implement climate responsive measures such as green infrastructures that mitigate urban heat, save energy and promote biodiversity in urban sustainability planning can increase the efficiency of coping with urban growth. The study highlights the key information on identifying the heat vulnerability zones, which are important to guiding the development of eco-friendly and sustainable infrastructure and urban policies for improving the livability and resiliency of city of Cuttack which is rapidly urbanizing.

Acknowledgements Authors are grateful to the Vice-Chancellor, Sambalpur University for providing necessary research facilities.

Author contributions Prasanta Kumar Patra: Conceptualization, Data curation Wrote the main manuscript text, data analysis, prepared maps. Duryadhan Behera: Writing—original draft, Vishal Chettry: Writing—original draft, Krishna Manjari Jena: Review and formatted the manuscript. Shreerup Goswami: Investigation, Methodology. Muralitharan Jothimani: Writing—original draft, Writing—review & editing.

Funding No specific funding has been received for this study.

Data availability Data is provided within the manuscript.

Declarations

Competing interests The authors declare no competing interests.

References

1. Shahfahad TS, Rihan M, Hang HT, Bhaskaran S, Rahman A. Modelling urban heat island (UHI) and thermal field variation and their relationship with land use indices over Delhi and Mumbai metro cities. Environ Dev Sustain. 2021;1:29. https://doi.org/10.1007/s10668-021-01587-7.
2. Sahak AS, Karsli F, Gormus KA. Seasonal monitoring of urban heat island based on the relationship between land surface temperature and land use/cover: a case study of Kabul City, Afghanistan. Earth Sci Inf. 2023;16:845–61. https://doi.org/10.1007/s12145-022-00918-0.
3. Chettry V. Geospatial analysis of urban sprawl in Agartala Municipal Council, India, from 1991 to 2021. Implementing the UN sustainable development goals—regional perspectives. Cham: Springer; 2023. https://doi.org/10.1007/978-3-030-91262-8_112-1.
4. Alsharif AA, Pradhan B, Mansor S, Shafri HZM. Urban expansion assessment by using remotely sensed data and the relative Shannon entropy model in GIS: a case study of Tripoli, Libya. Theoret Empir Res Urban Manag. 2015;10(1):55–71.
5. Willie YA, Pillay R, Zhou L, Orimoloye IR. Monitoring spatial pattern of land surface thermal characteristics and urban growth: a case study of King Williams using remote sensing and GIS. Earth Sci Inf. 2019;12:447–64. https://doi.org/10.1007/s12145-019-00391-2.
6. Chatterjee T, Behera D, Goswami S, Patra P. Delineation of groundwater potential zones in Kotagarh block of kandhamal District, Odisha through geospatial technique. Environ Qual Manag. 2023. https://doi.org/10.1002/tqem.22157.
7. Jha P, Joy MS, Yadav PK, Begam S, Bansal T. Detecting the role of urban green parks in thermal comfort and public health for sustainable urban planning in Delhi. Discov Public Health. 2024;21:236. https://doi.org/10.1186/s12982-024-00368-7.
8. Denge Y, Srinivashan S. Urban land use change and regional access: a study in Beijing, China. Habitat Int. 2016;51:103–13. https://doi.org/10.1016/j.habitatint.2015.09.007.
9. Chettry V. Geospatial measurement of urban sprawl using multi-temporal datasets from 1991 to 2021: case studies of four Indian medium-sized cities. Environ Monit Assess. 2022;194:860. https://doi.org/10.1007/s10661-022-10542-6.
10. Singh P, Kikon N, Verma P. Impact of land use change and urbanization on urban heat Island in Lucknow City, central India. A remote sensing based estimate. Sustain Cities Soc. 2017;32:100–14. https://doi.org/10.1016/j.scs.2017.02.018.
11. Patra PK, Behera D, Goswami S, Chatterjee T, Jena KM. Markov model decodes Cuttack's Landscape shifts: geospatial insights into urban metamorphosis. Environ Qual Manag. 2024. https://doi.org/10.1002/tqem.22303.
12. Patra PK, Behera D, Goswami S. Relative Shannon's entropy approach for quantifying urban growth using remote sensing and Gis: a case study of Cuttack City, Odisha, India. J Indian Soc Remote Sens. 2022;50:747–62. https://doi.org/10.1007/s12524-022-01493-z.
13. Ho HC, Knudby A, Xu Y, Hodul M, Aminipouri M. A comparison of urban heat islands mapped using skin temperature, air temperature, and apparent temperature (Humidex), for the greater Vancouver area. Sci Total Environ. 2016;544:929–38. https://doi.org/10.1016/j.scitotenv.2015.12.021.
14. Wang A, Zhang M, Kafy A, Tong B, Hao D, Yanfei F. Predicting the impacts of urban land change on LST and carbon storage using InVEST, CA-ANN and WOA-LSTM models in Guangzhou, China. Earth Sci Inf. 2023;16:437–54. https://doi.org/10.1007/s12145-022-00875-8.
15. Estoque RC, Murayama Y, Myint SW. Effects of landscape composition and pattern on land surface temperature: an urban heat island study in the megacities of Southeast Asia. Sci Total Environ. 2016;577:349–59. https://doi.org/10.1016/j.scitotenv.2016.10.195.
16. Dhole A, Kadaverugu R, Tomar Biniwale R, Sharma A. Impact of land cover classes on surface temperature in the vicinity of urban lakes and vegetation patches: a non-parametric regression analysis over decadal data. Earth Sci Inf. 2023. https://doi.org/10.1007/s12145-023-01140-2.
17. EPA (US Environmental Protection Agency). Reducing urban heat Islands: compendium of strategies. Washington, DC: US Environmental Protection Agency; 2008.
18. Kikon N, Singh P, Singh SK, Vyas A. Assessment of urban heat islands (UHI) of Noida City, India using multi-temporal satellite data. Sustain Cities Soc. 2016;22:19–28. https://doi.org/10.1016/j.scs.2016.01.005.
19. Liu L, Zhang Y. Urban heat island analysis using the landsat TM data and ASTER data: a case study in Hong Kong. Remote Sens. 2011;3(7):1535–52. https://doi.org/10.3390/rs3071535.
20. Patra PK, Behera D, Naik SP, Goswami S. Spatiotemporal variation of vegetation and urban sprawl using remote sensing and GIS: a case study of Cuttack City, Odisha, India. J Geosci Res. 2021;6(2):213–9.

21. Chatterjee T, Behera D, Goswami S, Patra PK, Munshi S. Appraisal of hydrochemical quality of groundwater in bamanghaty subdivision of Mayurbhanj District, Odisha, India using geospatial technology. J Geosci Res. 2022;7(2):209–15.
22. Shahmohamadi P, Che-Ani AI, Etessam I, Maulud KNA, Tawil NM. Healthy environment: the need to mitigate urban heat island effects on human health. Procedia Eng. 2011;20:61–70. https://doi.org/10.1016/j.proeng.2011.11.139.
23. Nikkala S, Peddada JR, Neredimelli R. Correlation analysis of land surface temperature on landsat-8 data of Visakhapatnam Urban Area, Andhra Pradesh, India. Earth Sci Inf. 2022;15:1963–75. https://doi.org/10.1007/s12145-022-00850-3.
24. Norton BA, Coutts AM, Livesley SJ, Harris RJ, Hunter AM, Williams NS. Planning for cooler cities: a framework to prioritise green infrastructure to mitigate high temperatures in urban landscapes. Landsc Urban Plan. 2015;134:127–38. https://doi.org/10.1016/j.landurbplan.2014.10.018.
25. Bai L, Woodward A, Liu Q. County-level heat vulnerability of urban and rural residents in Tibet, China. Environ Health. 2016;15(1):3. https://doi.org/10.1186/s12940-015-0081-0.
26. Mourya M, Kumari B, Tayyab M, Paarcha A, Rahman A. Indices based assessment of built-up density and surban expansion of fast-growing Surat city using multi-temporal Landsat data sets. GeoJournal. 2021;86(4):1607–23. https://doi.org/10.1007/s10708-020-10148-w.
27. Halder B, Bandyopadhyay J, Khedher KM, Fai CM, Tangang F, Yaseen ZM. Delineation of urban expansion influences urban heat islands and natural environment using remote sensing and GIS-based in industrial area. Environ Sci Pollut Res. 2022;29(48):73147–70. https://doi.org/10.1007/s11356-022-20821-x.
28. Navarro-Estupiñan J, Robles-Morua A, Díaz-Caravantes R, Vivoni ER. Heat risk mapping through spatial analysis of remotely-sensed data and socioeconomic vulnerability in Hermosillo. México Urban Climate. 2019;31: 100576. https://doi.org/10.1016/j.uclim.2019.100576.
29. Uejio CK, Wilhelmi OV, Golden JS, Mills DM, Gulino SP, Samenow JP. Intra-urban societal vulnerability to extreme heat: the role of heat exposure and the built environment, socioeconomics, and neighborhood stability. Health Place. 2011;17(2):498–507.
30. Oven KJ, Curtis SE, Reaney S, Riva M, Stewart MG, Ohlemüller R, Holden R. Climate change and health and social care: defining future hazard, vulnerability and risk for infrastructure systems supporting older people's health care in England. Appl Geogr. 2012;33:16–24.
31. Kadaverugu RA. Comparison between WRF-simulated and observed surface meteorological variables across varying land cover and urbanization in south-central India. Earth Sci Inf. 2023;16:147–63. https://doi.org/10.1007/s12145-022-00927-z.
32. Aubrecht C, Ozceylan D. Identification of heat risk patterns in the US National capital region by integrating heat stress and related vulnerability. Environ Int. 2013;56:65–77. https://doi.org/10.1016/j.envint.2013.03.005.
33. Zhu Q, Liu T, Lin H, Xiao J, Luo Y, Zeng W, Ma W. The spatial distribution of health vulnerability to heat waves in Guangdong Province, China. Global Health Act. 2014;7(1):25051. https://doi.org/10.3402/gha.v7.25051.
34. Nandi S, Gamkhar S. Urban challenges in India: a review of recent policy measures. Habitat Int. 2013;39:55–61. https://doi.org/10.1016/j.habitatint.2012.10.001.
35. Swain BK, Goswami S. Analysis and appraisal of urban road traffic noise of the City of Cuttack, India. Pakistan J Sci Indust Res Series A Phys Sci. 2014;57(1):10–9.
36. Swain BK, Goswami S. A study on noise in Indian banks: an impugnation in the developing countries: noise study in Indian banks. Pakistan J Sci Indust Res Series A Phys Sci. 2014;57(2):103–8.
37. Hadjimitsis DG, Clayton CRI, Hope VS. An assessment of the effectiveness of atmospheric correction algorithms through the remote sensing of some reservoirs. Int J Remote Sens. 2004;25:3651–74.
38. Duda RO, Hart PE, Stork DG. Pattern classification. 2nd ed. Hoboken: Wiley- Interscience Publication; 2000.
39. Lillesand TM, Kiefer RW, Chipman JW. Remote sensing and image interpretation. 6th ed. Hoboken: John Wiley and Sons publication; 2012.
40. Alkaradaghi K, Ali SS, Al-Ansari N, Laue J. Land use classification and change detection using multi-temporal Landsat imagery in Sulaimaniyah Governorate, Iraq. Conf Arab J Geosci. 2019. https://doi.org/10.1007/978-3-030-01440-7_28.
41. Butt AS, Shabbir R, Ahmad S, Aziz N. Land use change mapping and analysis using remote sensing and GIS: a case study of Simly watershed, Islamabad, Pakistan. Egypt J Remote Sens Space Sci. 2015;18(2):251–9.
42. Bhatta B. Analysis of urban growth pattern using remote sensing and GIS: a case study of Kolkata, India. Int J Remote Sens. 2009;30(18):4733–46. https://doi.org/10.1080/01431160802651967.
43. Stathopoulou M, Synnefa A, Cartalis C, Santamouris M, Karlessi T, Akbari H. A surface heat island study of Athens using high-resolution satellite imagery and measurements of the optical and thermal properties of commonly used building and paving materials. Int J Sustain Energ. 2009;28:59–76. https://doi.org/10.1080/14786450802452753.
44. Ahmed S. Assessment of urban heat islands and impact of climate change on socioeconomic over Suez Governorate using remote sensing and GIS techniques. Egypt J Remote Sens Space Sci. 2018;21(1):15–25. https://doi.org/10.1016/j.ejrs.2017.08.001.
45. Faisal AA, Kafy AA, Rakib AA, Akter KS, Jahir DMA, Sikdar MS, Ashrafi TJ, Mallik S, Rahman MM. Assessing and predicting land use/land cover, land surface temperature and urban thermal field variance index using Landsat imagery for Dhaka Metropolitan area. Environ Chall. 2021. https://doi.org/10.1016/j.envc.2021.100192.
46. Van TT, Bao HDX. Study of the impact of urban development on surface temperature using remote sensing in Ho Chi Minh City, North Vietnam. Geogr Res. 2010;48(1):86–96. https://doi.org/10.1111/j.1745-5871.2009.00607.x.
47. Al Kuwari NY, Ahmed S, Kaiser MF. Optimal satellite sensor selection utilized to monitor the impact of urban sprawl on the thermal environment in Doha City, Qatar. J Earth Sci Clim Change. 2016;7:326. https://doi.org/10.4172/2157-7617.1000326.
48. Joy MS, Jha P, Yadav PK, Bansal T, Rawat P, Begam S. Site suitability analysis of urban green parks in Ranchi city using GIS–AHP based multi-criteria decision analysis. Urban Sustain Soc. 2024;1(1):169–98. https://doi.org/10.1108/uss-10-2023-0008.
49. Gomez FR, Canero RF, Perez G, Avila JC, RodrIguez DL, Urrestarazu LP. Detection of unfavourable urban areas with higher temperatures and lack of green spaces using satellite imagery in sixteen Spanish cities. Urban Forest Urban Green. 2022. https://doi.org/10.1016/j.ufug.2022.127783.
50. Tan KC, Lim HS, Matjafri MZ, Abdullah K. Landsat data to evaluate urban expansion and determine land use/land cover change in Penang Island, Malays. Environ Earth Sci. 2010;60:1509–21.
51. Xiong Y, Huang S, Chen F, Ye H, Wang C, Zhu C. The impacts of rapid urbanization on the thermal environment: a remote sensing study of Guangzhou, South China. Remote Sens. 2012;4(7):2033–56. https://doi.org/10.3390/rs4072033.

52. Yue W, Liu Y, Fan P, Ye X, Wu C. Assessing spatial pattern of urban thermal environment in Shanghai, China. Stochastic Environ Res Risk Assess. 2012;26:899–911. https://doi.org/10.1007/s00477-012-0638-1.
53. Javaid K, Ghafoor GZ, Sharif F, et al. Spatio-temporal analysis of land use land cover change and its impact on land surface temperature of Sialkot City, Pakistan. Sci Rep. 2023;13:22166. https://doi.org/10.1038/s41598-023-49608-x.
54. Isinkaralar O. QGIS-based modeling and analysis of urban dynamics affecting land surface temperature towards climate hazards in coastal zones of Portugal. Nat Hazards. 2024;120:7749–64. https://doi.org/10.1007/s11069-024-06519-y.
55. Negesse MD, Hishe S, Getahun K. Urban land use, land cover change and urban microclimate dynamics in Addis Ababa. Ethiopia Discov Environ. 2024;2:71. https://doi.org/10.1007/s44274-024-00105-6.
56. Aiymeku TG, Tabor KW, Wedajo GD, Zenebe RR. Green spaces suitability analysis for urban resilience using geospatial technology: the case of Jimma city, Oromia, Ethiopia. Environ Dev Sustain. 2024. https://doi.org/10.1007/s10668-023-04365-9.
57. Badugu A, Arunab KS, Mathew A. Predicting land surface temperature using data-driven approaches for urban heat island studies: a comparative analysis of correlation with environmental parameters. Model Earth Syst Environ. 2024;10:1043–76. https://doi.org/10.1007/s40808-023-01822-2.
58. Gohain KJ, Goswami A, Mohammad P, Kumar S. Modelling relationship between land use land cover changes, land surface temperature and urban heat island in Indore city of central India. Theoret Appl Climatol. 2023;151:1981–2000. https://doi.org/10.1007/s00704-023-04371-x.
59. Sangwan A, Ananad V, Kumar N, Kumar A, Jat MK, Ahmed R. Development of site suitability framework for urban greenspace: a case study of Sikar city, Rajasthan, India. Environ Earth Sci. 2024;83:634. https://doi.org/10.1007/s12665-024-11898-3.
60. Manna H, Sarkar S, Hossain M, Dolui M. Modeling and predicting spatio-temporal Land use land cover changes and urban sprawling in Kalaburagi City Corporation, Karnataka, India: a geospatial analysis. Modeling Earth Syst Environ. 2023. https://doi.org/10.1007/s40808-023-01814-2.
61. Zheng H, Chen Y, Wei P, Cai Y, Chen Z. Impact of land use/land cover changes on the thermal environment in urbanization: a case study of the natural wetlands distribution area in Minjiang River Estuary, China. Polish J Environ Stud. 2019;28(4):3025–41. https://doi.org/10.15244/pjoes/93743.
62. Anupriya RS, Rubeena TA. Spatio-temporal urban land surface temperature variations and heat stress vulnerability index in Thiruvananthapuram city of Kerala, India. Geol Ecol Landscapes. 2023. https://doi.org/10.1080/24749508.2023.2182088.
63. Neog R. Mapping the heat stress vulnerability landscape of Agartala City, India. GeoJournal. 2024. https://doi.org/10.1007/s10708-024-11072-z.